

Dynamic Modulation of Electromagnetically Induced Transparency Metamaterials through Mode Coupling and Stretchable Design

Sihong Chen, *Member, IEEE*, Taisong Pan, Zhengcheng Mou, Bing-Zhong Wang, *Senior Member, IEEE*, and Yuan Lin

Abstract—The active control of electromagnetically induced transparency (EIT) metamaterials (MM) has the potential to revolutionize communication networks without relying on quantum technology. However, current reconfigurable systems offer limited flexibility and have high fabrication costs and difficulties. In this study, we examine a classical EIT metamaterial and discover a novel modulation mechanism that leverages mode coupling to dynamically adjust the bandwidth and group delay of the EIT MM. This mechanism is verified through analyses of the electric field and surface charge density distributions. Additionally, a robust coupled Lorentz oscillator model is used to explain the coupling mechanism, with results that are in good agreement with simulations and experiments. To capitalize on this mechanism, we propose a block-definition approach where the MM is divided into stretchable sections, allowing for dynamic modulation of the bandwidth and group delay by stretching the EIT MM. Furthermore, the fabrication process is highly compatible with traditional flexible printed circuit board techniques. Our block-definition EIT MM offers unprecedented tunability and flexibility, requiring no complex components or specialized materials, making it a promising candidate for tunable slow-wave devices and other reconfigurable microwave applications.

Index Terms—Electromagnetically induced transparency, mode coupling, stretchable metamaterials, block-definition, group delay and bandwidth modulation.

I. INTRODUCTION

Metamaterials (MMs) provide a diverse and incredible way to manipulate electromagnetic waves, making them widely used in sensing [1], [2], electromagnetic cloaking [3], perfect absorption [4]–[7], hologram imaging [8] and polarization conversion [9]. The phenomenon of electromagnetic induced transparency (EIT) is a quantum interference effect that creates

a window of transmission within the absorption band of a three-level atomic system [10]. This leads to extreme modifications in dispersion characteristics and can have many potential applications, such as slow light [11]–[13] and enhanced non-linear effects [14], [15]. However, achieving this effect through conventional quantum EIT methods requires harsh experimental conditions. To overcome this limitation, the use of MMs has been proposed to mimic the original quantum EIT effect [16]–[26].

As a result, various MM-based EIT applications have been reported [27]–[37], with slow-light devices being one of the most significant [32]–[34]. The delay-bandwidth product (DBP) is a critical metric that measures the performance of slow light, as it is the product of the maximum group delay and full width at half maximum (FWHM) bandwidth [38], [39]. To achieve good results in slow light, it is important to have a large group delay time and bandwidth for EIT MMs. However, the EIT effects based on MMs have a very narrow transmission window due to their intrinsic resonant characteristics [16].

Although there have been some reports demonstrating broadband EIT effects in terahertz and optical regime [16], [40], [41], the quest for new designs to achieve a transparent window over a broad spectral range is still urgent and remains a challenging issue, especially in the low-frequency regions. Additionally, in some situations, real-time reconfigurability is needed in response to rapidly varying operational scenarios, but conventional EIT MMs cannot meet these requirements. Their fixed properties seriously hamper the developments and practical applications of EIT effects. Some efforts have been made to modify the EIT effect in MMs through hybrid EIT MMs [42]–[48] and MEMS reconfigurable EIT MMs [49]–[51]. However, in these strategies, the active control of EIT effect is basically achieved by integrating adjustable materials and components or adopting tedious preparation processes, which increases costs and hinders their applications. Also, these strategies are not suitable for the applications in microwave applications, as they require large areas of adjustable materials and components, and the fabrication of large-area reconfigurable MEMS-based MMs is a challenge.

Recently, stretchable devices, implemented on polymers with low surface energy, can attach to arbitrary surfaces in a conformal manner [52], [53]. This flexibility allows for the integration of passive or functional devices with curved surfaces and packaging materials, unlike rigid platforms. This new development in MMs opens up the possibility for recon-

Sihong Chen is with the School of Materials and Energy, School of Physics, University of Electronic Science and Technology of China, Chengdu 610054, China, and also with Huawei Technologies, Chengdu 610041, China (e-mail: Sihongchen@outlook.com or chensihong1@huawei.com).

Taisong Pan is with the School of Materials and Energy, University of Electronic Science and Technology of China, Chengdu 610054, China (e-mail: tspan@uestc.edu.cn).

Zhengcheng Mou is with the School of Statistics, Southwestern University of Finance and Economics, Chengdu 611130, China (e-mail: mzc971123@foxmail.com).

Bing-Zhong Wang is with the Institute of Applied Physics, University of Electronic Science and Technology of China, Chengdu 611731, China (e-mail: bzhwang@uestc.edu.cn).

Yuan Lin is with the School of Materials and Energy, Medico-Engineering Cooperation on Applied Medicine Research Center, University of Electronic Science and Technology of China, Chengdu 610054, China (e-mail: linyuan@uestc.edu.cn).

Corresponding author: Taisong Pan

figurable or multi-functional devices.

Thus, in this paper, we introduce a new modulation mechanism that utilizes mode coupling tuning to achieve reconfigurable bandwidth and group delay in EIT analogue. This new mechanism was inspired by stretchable MMs. After a comprehensive analysis of a classical EIT structure, we uncovered the new modulation mechanism and demonstrated it with the help of a robust coupled Lorentz oscillator mode, which showed good alignment with simulations and confirmed by the analysis of electric field and surface charge density distributions. Prototype devices were also fabricated and tested, with results consistent with simulations. To realize dynamic modulation of the frequency response and group delay, we proposed defining the devices into stretchable blocks using transfer printing and laser cutting techniques. Both simulations and experiments indicate that the group delay and bandwidth can be adjusted in a continuous manner by stretching the device. The proposed EIT MM fabrication process is compatible with traditional flexible PCB techniques and does not require complex components or specialized materials. This approach has great potential for tunable slow-wave devices and other microwave tunable devices, offering on-the-fly tunability and high flexibility for various specifications such as microwave buffering and active filtering.

II. DESIGN CONCEPT OF THE EIT MMs

The schematic illustration of the analyzed MMs is presented in Fig. 1(a), which employed a kind of classical structure to produce the EIT-like effect, similar to the reference reported by Jianqiang Gu *et al.* [42]. The unit cell of 0.018 mm-thick copper (Cu)-based structure consists of a cut wire (CW) and two split-ring resonators (SRRs) fabricated on flexible polyimide substrate (relative permittivity: 3.5, loss tangent: 0.008 and thickness: 0.1 mm). The lattice constant of array is $P_x = P_y = 16$ mm and the length and width of the CW is $L = 11$ mm and $w = 0.5$ mm, respectively. We use d_x to describe the coupling distance between the SRRs and CW with a initial value $d_x = 2.0$ mm. The SRRs are $h = 3.5$ mm in side length and $g = 0.5$ mm in split gap and the $d_y = 5$ mm represents the distance between the SRRs. To clarify the EIT analogue of the MMs in microwave region, three sets of arrays are simulated with the unit cell composed of a CW, a pair of SRRs and both of them, respectively, and the corresponding transmission responses are shown in Fig. 1(b). It can be seen that the CW exhibits a typical electric resonance at 11.5 GHz [16], [54], which has a broad line width because of the strong radiation losses under the normal incident plane wave with the electric field parallel to it, whereas the SRRs, supporting an LC resonance mode with a narrow line width at the same frequency, are inactive due to the incident electric field perpendicular to the structure. When both of them are arranged into the unit cell, the field coupling will occur between the CW and the SRR-pair, in which the CW that exhibits electric resonance and the SRRs that excite the LC resonance serve as the bright and dark mode, respectively. The destructive interference between the electric resonance and LC resonance leads to appearance of the EIT-like behavior. Fig. 1(c) demonstrates the design concept of

dynamic modulation of frequency response and group delay of the device. Vector Network Analyzer (VNA) is used to test the transmission response of the proposed devices, to which two ridge antennas are connected to the VNA and placed in the line of sight to each other with the fabricated device placed in the middle. The frequency response and group delay of the device can be continuously modulated by controlling the coupling distance of stretchable EIT MMs with a customized stretching holder.

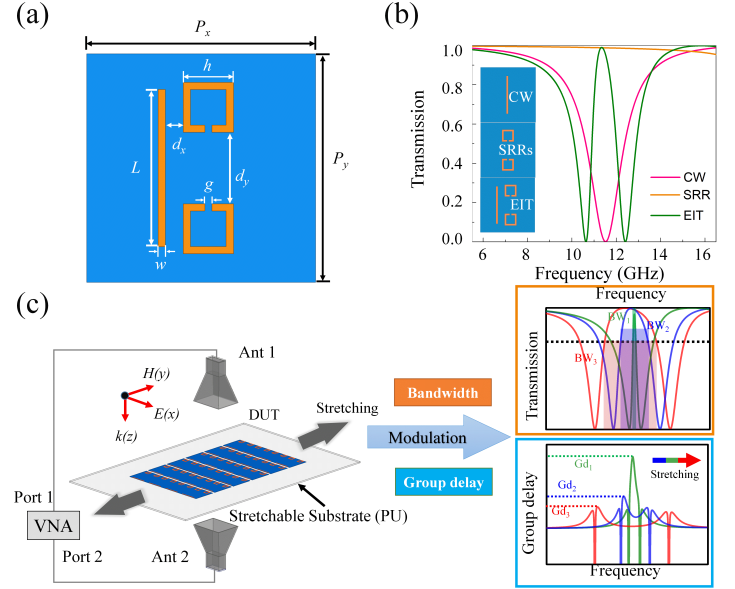


Fig. 1. (a) The geometrical illustration of the proposed EIT MM. The relevant geometrical parameters are as follows: $P_x = P_y = 16$ mm, $d_x = 2.0$ mm, $h = 3.5$ mm, $g = 0.5$ mm, $d_y = 5$ mm, $w = 0.5$ mm and $L = 11$ mm. (b) Simulated transmission response of the CW, SRRs and EIT MM. Insets show the geometries of the CW, the SRRs and the EIT MM, respectively. (c) Experimental setup of the EIT MM and corresponding demonstration of its modulation effect on bandwidth and group delay with stretching.

III. ANALYSES OF THE EIT MMs

To verify the feasibility of the design concept, we did detailed analyses on the proposed structures. The full-wave numerical simulation software CST Microwave Studio is employed to analyze the spectral response, as shown in Fig. 2. In these calculations, open boundary conditions are set along the electromagnetic wave propagating direction (z-direction), and periodic boundary conditions are applied to mimic the function of a 2D infinite condition. As discussed in previously reports [55], the coupling mechanism between the SRRs and CW plays a key role in controlling the EIT effect. Thus, we firstly studied the transmission characteristics with different coupling distance (d_x), as demonstrated in Fig. 2. By tuning the coupling distance (d_x), we plot the transmission amplitude and phase, group delay and group index for a set of MMs with different d_x . As we can see that there is a strong correlation between the bandwidth and group delay of EIT effect and coupling distance, in which the bandwidth of the EIT narrows with the increase of d_x , along with a gradually increase of the max group delay and group index. Notably, the disappearance

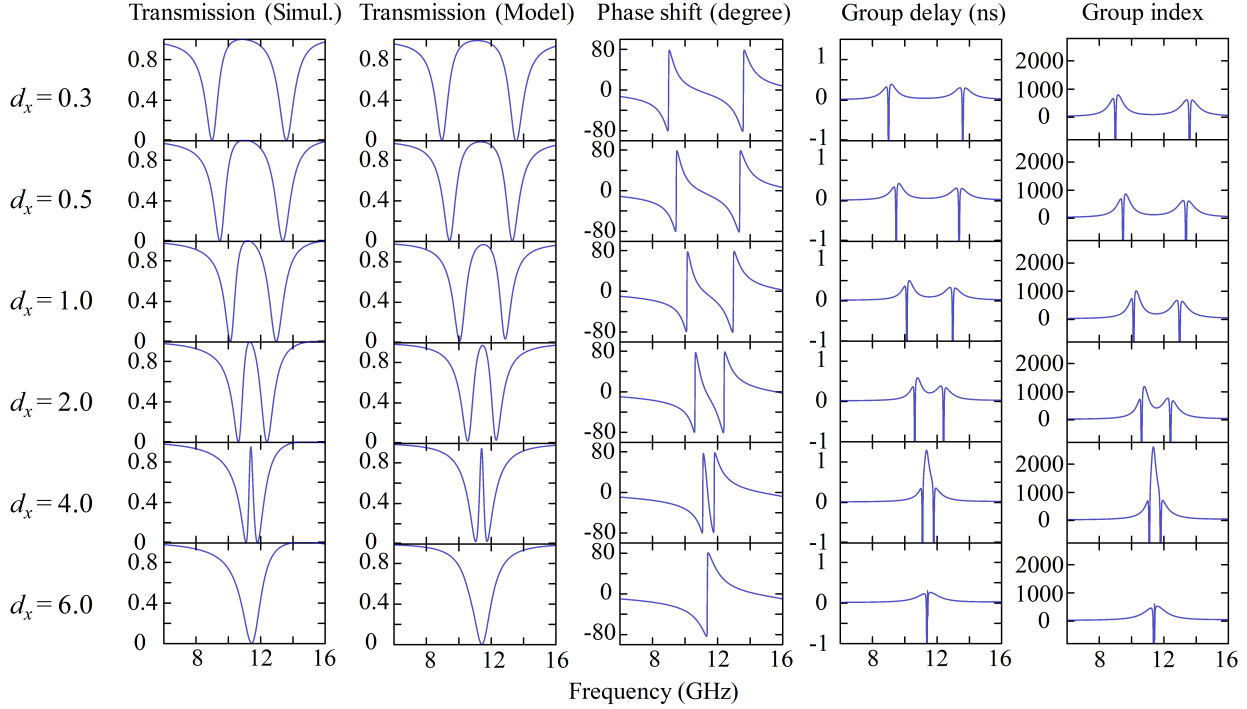


Fig. 2. Spectra of the transmission amplitude (simulation and coupled Lorentz oscillator model) and phase, group delay and group index of EIT MM with different coupling distance.

of the transmission window is observed at the d_x of 6 mm, with the same situation of group delay.

To explore the physical mechanism of this behavior, we employed the coupled Lorentz oscillator model to quantitatively explain the near field coupling between the bright and dark mode with the change of d_x [18], [55]. Similar to quantum EIT in the three-level system, we employed a ground state $|0\rangle$ and two excited states $|1\rangle$ and $|2\rangle$ to illustrate the model, of which the transitions $|0\rangle - |1\rangle$ and $|0\rangle - |2\rangle$ represent the dipole-allowed transition and dipole-forbidden transition, corresponding to the typical dipole bright mode resonance in the CW and the LC dark mode resonance in the SRRs, respectively. Then, the transition between $|1\rangle$ and $|2\rangle$ illustrates the coupling between the CW and the SRRs. Because there exist two possible excitation pathways of $|0\rangle - |1\rangle$ and $|0\rangle - |1\rangle - |2\rangle - |1\rangle$, introducing destructive interference, which leads to strong suppression of loss and large dispersion within a narrow frequency band. The interference in the MMs can be analytically described by the coupled differential equations [16], [56], [57],

$$\ddot{x}_1(t) + \gamma_1 \dot{x}_1(t) + \omega_0^2 x_1(t) + \Omega x_2(t) = g E_0(t) \quad (1)$$

$$\ddot{x}_2(t) + \gamma_2 \dot{x}_2(t) + (\omega_0 + \delta)^2 x_2(t) + \Omega x_1(t) = 0. \quad (2)$$

Where x_1 and x_2 represent the amplitudes and γ_1 and γ_2 describe the radiating rate of bright and dark mode, respectively. Then the parameter g describes the coupling strength between the bright mode and the incident electromagnetic field and the coupling coefficient between the resonators is represented by Ω . The difference between resonance frequency of intrinsic

oscillators and transparency frequency is described by the detuning factor δ . By solving the coupled equations 1 and 2 using the displacement vector $\mathbf{x}_n(t) = x_n e^{i\omega t}$ ($n = 1, 2$) and the approximation $\omega_1^2 - \omega^2 \approx -2\omega_1(\omega - \omega_1)$ [21], we can get the transmission coefficient based on the relation of $T = 1 - R$ [58].

$$T = 1 - \text{Re} \frac{\text{ig}^2(\omega - \omega_0 - \delta + i\gamma_2/2)}{(\omega - \omega_0 + i\gamma_1/2)(\omega - \omega_0 - \delta + i\gamma_2/2) - \Omega^2/4}. \quad (3)$$

The analytical modeled transmission data using the equation 3 are presented in Fig. 2 (Transmission Model), which exhibits good agreements with the simulations. The corresponding fitting parameters are listed in Table I and plotted in Fig. 3. It is observed that γ_1 , γ_2 and δ do not change significantly with the increase of d_x , whereas the coupling coefficient (Ω) decreases markedly, which indicates the coupled strength of the EIT MMs can be significantly tuned by changing the coupled distance d_x . Finally, with the increase of coupled distance, the coupling coefficient Ω becomes too small to excite the dark mode, which eventually results in the disappearance of the EIT transmission window.

TABLE I
THE FITTING PARAMETERS OF COUPLED LORENTZ OSCILLATOR MODEL.

d_x (mm)	γ_1 (GHz)	γ_2 (GHz)	Ω (GHz)	δ (GHz)	g
0.3	1.841	0.1488	4.587	-0.255	1.000
0.5	1.743	0.165	3.868	-0.0232	0.9753
1	1.633	0.1515	2.797	0.1611	0.9324
2	1.632	0.0667	1.744	0.0965	0.9099
4	1.563	0.0194	0.6914	0.03227	0.8797
6	1.414	0.979	0.3445	-0.5516	0.8555

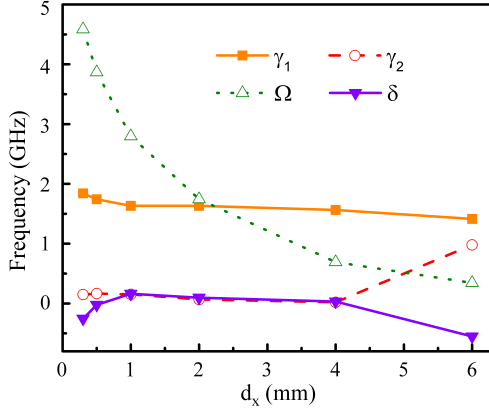


Fig. 3. The fitting parameters γ_1 , γ_2 , δ and Ω as a function of coupling distance d_x .

Furthermore, to figure out the coupling behavior of the proposed device, the electric field and surface charge density distributions at the resonance frequency are also presented to illuminate mode coupling process. Fig. 4 shows the distributions at different coupling distances ($d_x = 2.0$ mm, $d_x = 5.0$ mm, and $d_x = 6.0$ mm), corresponding to different coupling strength resulting in the pronounced EIT peak, EIT disappearance and only electric dipole resonance, respectively. As we can see in Fig. 4(a), when d_x is 2.0 mm, the electric field distributions are mainly concentrated around the SRRs' gap, whereas those in the CW are very weak. Meanwhile, in the analyzed structure, the incident waves cannot excite the LC resonance in the SRRs directly, so near-field coupling is the only way to excite LC resonance whose resonant frequency is the same with that of CW. When CW is excited by external waves, most of the energy is transferred to the SRRs by the electric field coupling, causing the suppression of the electric field in the CW, which is the characteristic of a typical EIT effect [18]. With the increase of d_x , the coupling strength gradually decreases and the electric field in the SRRs' gap is gradually suppressed, leading to a redistribution of the electric field in the EIT structures, as shown in Fig. 4(b), where the CW and SRRs are both excited. Then, as the continuous increase of the coupling distance, the electric field in the SRRs' gap is completely suppressed and the electric field distribution is primarily concentrated in the CW, as shown in Fig. 4(c), which behaves as a typical electric dipole resonance. Similar behaviors can be obtained in the distributions of surface current. Specifically, in Fig. 4(d), surface current is mainly concentrated on the SRRs in the strong coupling state ($d_x = 2$ mm). Then, as coupling distance increases to 5.0 mm, the surface current is redistributed to have both the SRR and CW excited with strong current flows shown in Fig. 4(e). With the further increase of coupling distance, the coupling disappears, so that the surface current is mostly focused on the CW, showing the typical characteristics of electric dipole resonance, as shown in Fig. 4(f). Thus, the origin of modulation of EIT resonance is realized by tuning the coupling strength, namely, by changing the distance between the SRRs and CW.

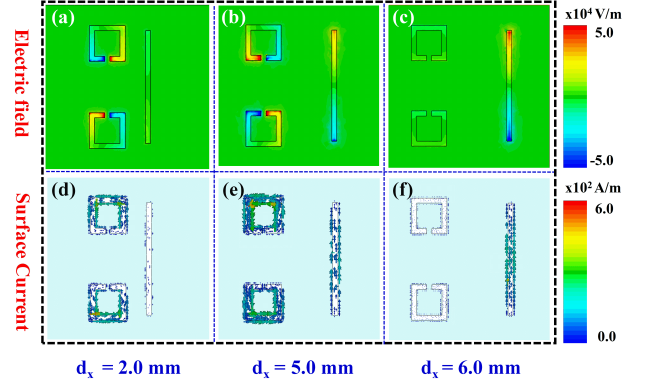


Fig. 4. The simulated electric field and surface charge density distributions at the resonance frequency (11.5 GHz) of the EIT MMIs with the coupling distance d_x of 2.0 mm, 5.0 mm and 6.0 mm, respectively.

To obtain a deep insight into the evolution of the transmittance and group delay as a function of the d_x , more calculations are presented. We map the two-dimensional transmission response spectra as a function of frequency as well as coupling distance at the step of 0.1 mm, as shown in Fig. 5(a). It shows that the transmission window gradually narrows with the increase of d_x , and the transmission amplitude is less than 0.7 at a distance greater than 5.4 mm. As is widely known, the prominent characteristics of the EIT phenomenon for slow-light devices are the product of the group delay time and bandwidth of transparency windows [59], [60]. Group delay (τ_g) can be calculated by

$$\tau_g = -\frac{\partial \phi}{\partial \omega}, \quad (4)$$

where ϕ is the transmission phase shift and ω is the angular frequency. The calculation of DBP can be calculated from the transmission FWHM bandwidth (Δf) and group delay as $DBP = \tau_g \times \Delta f$. Thus, we plotted the transmission bandwidth of the device with varied d_x at a transmission amplitude greater than 0.7 in Fig. 5(b), showing a decreasing trend from 3.68 to 0.01 GHz over the range from 0.3 to 5.4 mm. Then, a finer map of group delay as a function of frequency and d_x is simulated in Fig. 5(c) with the step of 0.1 mm as well. Negative group delay appears at the side of resonance modes, while an obviously positive group delay occurs over the transparency window and a increasing trend is observed. Thus, we extract the maximum group delay and plot it as a function of d_x into Fig. 5(d) marked with red sphere-symbol line. The achievement of maximum group delay is 17.14 ns at the d_x of 5.8 mm, but the transmission efficiency at the frequency is very small, thus being of little value for practical applications. Considering the transmission amplitude and group delay, the results of DBP with a transmission efficiency greater than 70% are shown in Fig. 5(d) with blue star-symbol line. The maximum DBP achieves 2.55 at the d_x of 1.3 mm.

To validate the simulated and modeled results, we fabricated four samples with different coupling distance, as presented in Fig. 6 and the simulated and experimental transmission and phase delay results are also demonstrated. As we can see,

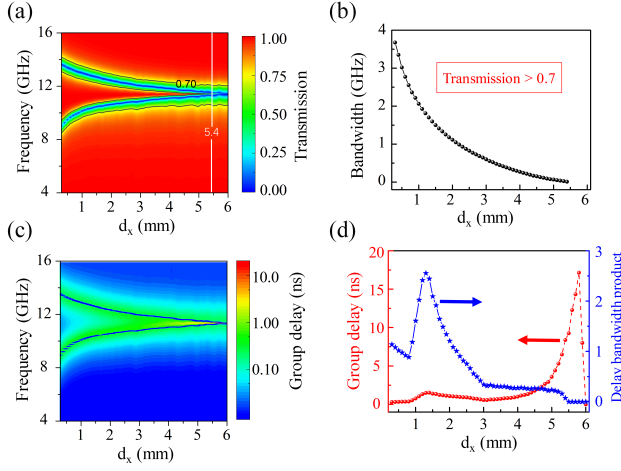


Fig. 5. (a) The simulated 2D map of transmission response spectra as a function of frequency as well as coupling distance. (b) Transmission bandwidth with amplitude greater than 0.7. (c) 2D map of group delay as a function of frequency as well as coupling distance. (d) The maximum group delay (red sphere-symbol line) and delay bandwidth product (blue star-symbol line) with the varied d_x . The step of d_x is 0.1 mm

there are good agreements between the experimental results with the simulated ones, which proves that the simulation and theoretical analysis are reasonable. Meanwhile, the results manifest that the bandwidth and group delay of EIT MMs can be tuned by adjusting the coupling distance to realize a broadband or narrow band EIT effect, or to suppress EIT effect.

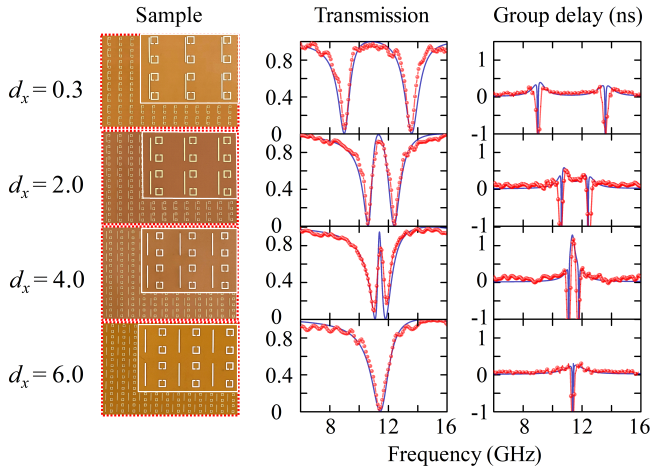


Fig. 6. The photographs of the fabricated EIT MM with different coupling distance d_x and the simulated (blue solid line) and experimental (red sphere-symbol line) transmission and phase delay results.

IV. DYNAMIC MODULATION OF THE EIT MMs

Inspired by stretchable MMs and above analyses, we introduced an approach based on transfer printing and laser cutting techniques to achieve the dynamic modulation of the bandwidth and group delay of EIT MMs. The detailed fabrication processes are demonstrated in Fig. 7. To fabricate the

tunable EIT device, the process starts from pasting the water-soluble tape onto EIT device based on the polyimide substrate, as show in Fig. 7 of step 1. The EIT device is fabricated on the flexible polyimide substrate using the traditional PCB technology. Then, in the step 2, the laser-cutting is used to define the tunable blocks of the EIT device. In this step, in order to ensure the integrity of the device, we need to accurately control the laser power, so that it can cut through PI layer without cutting through the water-soluble tape layer below. After that, we should transfer the device with defined blocks onto the stretchable substrate layer (Polyurethane, PU) and use the water to remove the water-soluble tape, as shown in step 3 and 4. At this point, the tunable function devices are obtained and can realize the tunability by mechanical loading (step 5).

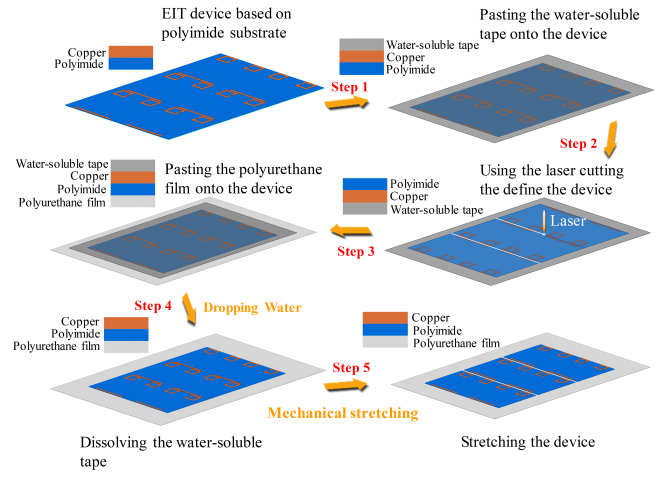


Fig. 7. The detailed fabrication process of stretchable EIT device based on the method of laser-cutting and transfer printing.

Then we measured the stretchable device with the experiment setup shown in Fig. 1(c), and presented the photos of five states with different stretching distance and corresponding simulated and experimental transmission and phase delay results in Fig. 8. The photos show a good control of the coupling distance in our measurement and the results also match well and demonstrate good modulation effects on the bandwidth and group delay by stretching the devices.

However, we found that the modulation range has a certain decrease compared with that in Fig. 6 due to the extension of P_x , making it difficult to achieve that only electric dipole resonance is excited within the stretching range of substrate. Hence, for the realization of expected modulation effect, we optimized the original structure. The original SRRs are replaced with a double splits resonator (DSR) structure to form a basic unit of the CW-DSR structure and the details are shown in Fig. 9.

Meanwhile, we also map the 2D transmission amplitude and phase delay spectra as a function of frequency as well as coupling distance under the condition of stretching loading at the step of 0.1 mm, as shown in Fig. 10(a) and Fig. 10(c). The similar trend is observed with the original design of the transmission bandwidth and group delay. The transmission

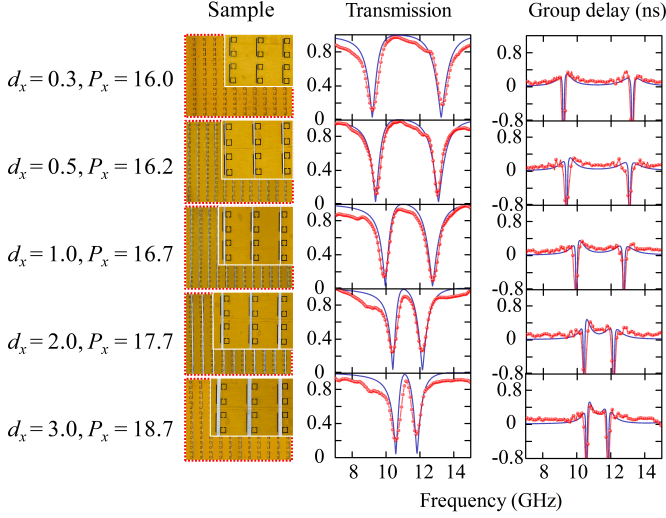


Fig. 8. The photographs of the tunable EIT MMs when stretched different distance and the simulated (blue solid line) and experimental (red sphere-symbol line) transmission and phase delay results.

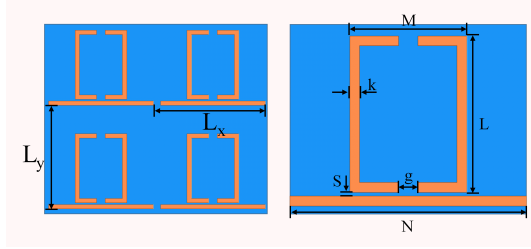


Fig. 9. Geometric illustration of the optimized EIT MM (CW-DSR). The detailed values are set to $L_x = 5.0$ mm, $L_y = 5.0$ mm, $M = 6.0$ mm, $N = 12.1$ mm, $L = 8.0$ mm, $k = 0.5$ mm and $g = 1.0$ mm. The initial gap between the DSR and CW resonator is $S = 0.2$ mm.

amplitude is greater than 0.7 when S is below 2.7 mm and the maximum group delay achieves 34.63 ns at the S of 2.7 mm, as shown in Fig. 10(b) and 10(d), respectively. Taking both transmission amplitude and group delay into consideration, the results of DBP with a transmission efficiency greater than 70% are shown in Fig. 10(d) with blue star-symbol line. The maximum DBP is 0.58 at the S of 0.2 mm.

To verify the simulation results, the prototype devices are fabricated using the same method in Fig. 7 and tested with the experimental setup in Fig. 1(c). The corresponding results are demonstrated in Fig. 11. By mechanically stretching, the coupling distance (S) can be controlled well as described in the photos. There are also good agreements of the transmission spectra between the simulated (blue solid line) and experimental (red sphere-symbol line) results with the stretching of S . Deterioration was observed in measured transmission amplitude and the value of maximum group delay caused by the fabrication tolerances and imperfections of measurement.

Then, compared the proposed structures with other reported EIT MMs within the GHz region in Table II, it can be seen that the DBP and group delay are greatly improved. Specifically, the bandwidth and group delay characteristics of the proposed design can be easily adjusted, which makes

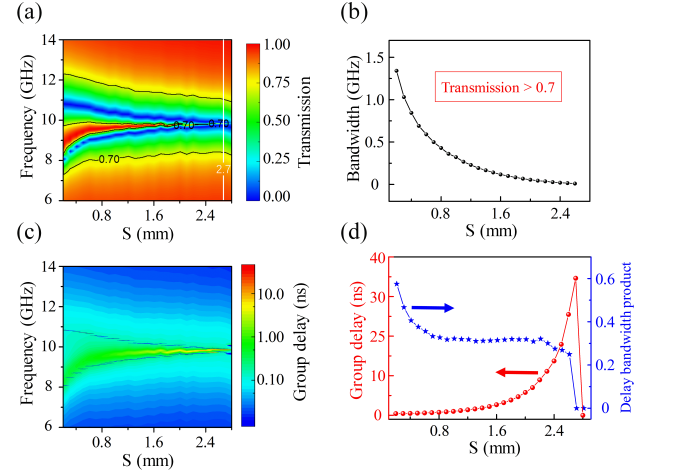


Fig. 10. (a) The simulated 2D map of transmission response spectra as a function of frequency as well as coupling distance (S). (b) Transmission bandwidth with amplitude greater than 0.7. (c) 2D map of group delay as a function of frequency as well as coupling distance at. (d) The maximum group delay (red sphere-symbol line) and delay bandwidth product (blue star-symbol line) with the varied S . The step of S is 0.1 mm

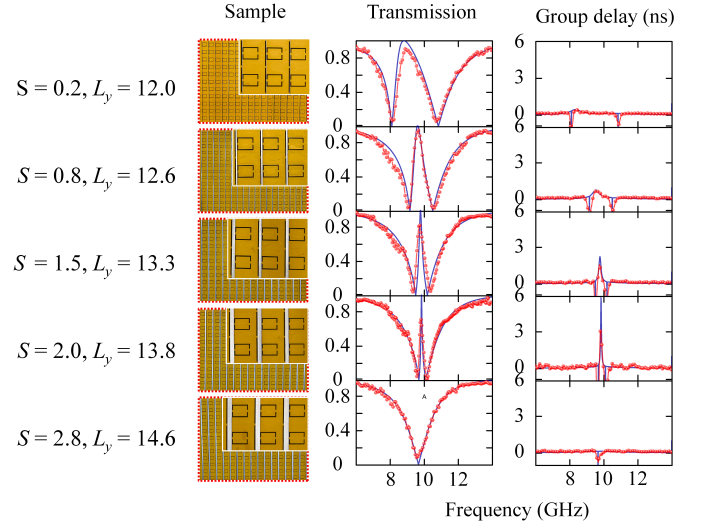


Fig. 11. The optical graphs of the fabricated improved EIT MM with the stretching of S and the simulated (blue solid line) and experimental (red sphere-symbol line) transmission and phase delay results.

great improvements in both dynamic regulation and slow wave characteristics.

V. CONCLUSION

In this study, we have discovered a novel way to modulate EIT MMs by analyzing the classical EIT structures, known as CW-SRRs. The proposed mechanism, based on mode coupling, enables reconfigurable bandwidth and group delay of the EIT effect. The underlying mechanism was described through the use of the coupled Lorentz oscillator model and demonstrated through the examination of electric field and surface charge density distributions. The results of our simulations and experiments were in good agreement. Furthermore, drawing

TABLE II
COMPARISON WITH PREVIOUS STUDIES OF EIT MMS IN MICROWAVE REGION.

Ref.	Transmission(a.u)	Group delay(ns)	DBP	Polarization dependency	Tunability(Y/N)
[61]	0.78	1.46	-	dependent	N
[39]	0.72	2.4	0.39	dependent	N
[62]	0.70	0.333	0.45	independent	N
[63]	0.728	0.708	0.505	independent	N
[64]	0.81	0.83	-	independent	N
[65]	-	-	0.528	dependent	N
CW-SRRs	0.70	1.5	2.55	dependent	Y
CW-DSR	0.70	0.43	0.58	dependent	Y

inspiration from the tuning mechanism, we presented a block definition design to create stretchable EIT MMs through transfer printing and laser cutting techniques. This approach allowed us to dynamically modulate the bandwidth and group delay of the EIT effect with a large DBP of up to 2.55. In addition, by optimizing the structure design, we proposed CW-DSRs to achieve dynamic modulation of the broadband, narrowband, and suppression of the EIT effect, simply by stretching the device. The ease of fabrication, simplicity of modulation, and compatibility with large-area implementation, make the proposed EIT MM a promising candidate for tunable slow-wave devices and microwave switches.

ACKNOWLEDGMENT

This work is supported by the National Natural Science Foundation of China (Nos. 61825102, 52021001, and 61901085), and Medico-Engineering Cooperation Funds from University of Electronic Science and Technology of China (No. ZYGX2021YGLH008)

REFERENCES

- [1] L. Cong, S. Tan, R. Yahiaoui, F. Yan, W. Zhang, and R. Singh, "Experimental demonstration of ultrasensitive sensing with terahertz metamaterial absorbers: A comparison with the metasurfaces," *Applied Physics Letters*, vol. 106, no. 3, p. 031107, 2015. [Online]. Available: <https://doi.org/10.1063/1.4906109>
- [2] R. Yahiaoui, A. C. Strikwerda, and P. U. Jepsen, "Terahertz plasmonic structure with enhanced sensing capabilities," *IEEE Sensors Journal*, vol. 16, no. 8, pp. 2484–2488, April 2016.
- [3] D. Schurig, J. J. Mock, B. J. Justice, S. A. Cummer, J. B. Pendry, A. F. Starr, and D. R. Smith, "Metamaterial electromagnetic cloak at microwave frequencies," *Science*, vol. 314, no. 5801, pp. 977–980, 2006. [Online]. Available: <http://science.sciencemag.org/content/314/5801/977>
- [4] N. I. Landy, S. Sajuyigbe, J. J. Mock, D. R. Smith, and W. J. Padilla, "Perfect metamaterial absorber," *Phys. Rev. Lett.*, vol. 100, p. 207402, May 2008. [Online]. Available: <https://link.aps.org/doi/10.1103/PhysRevLett.100.207402>
- [5] C. M. Watts, X. Liu, and W. J. Padilla, "Metamaterial electromagnetic wave absorbers," *Advanced Materials*, vol. 24, no. 23, pp. OP98–OP120, 2012. [Online]. Available: <https://onlinelibrary.wiley.com/doi/abs/10.1002/adma.201200674>
- [6] R. Alaei, M. Farhat, C. Rockstuhl, and F. Lederer, "A perfect absorber made of a graphene micro-ribbon metamaterial," *Opt. Express*, vol. 20, no. 27, pp. 28 017–28 024, Dec 2012. [Online]. Available: <http://www.opticsexpress.org/abstract.cfm?URI=oe-20-27-28017>
- [7] H. Li, L. H. Yuan, B. Zhou, X. P. Shen, Q. Cheng, and T. J. Cui, "Ultrathin multiband gigahertz metamaterial absorbers," *Journal of Applied Physics*, vol. 110, no. 1, p. 014909, 2011. [Online]. Available: <https://doi.org/10.1063/1.3608246>
- [8] G. Zheng, H. Mühlenbernd, M. Kenney, G. Li, T. Zentgraf, and S. Zhang, "Metasurface holograms reaching 80% efficiency," *Nature nanotechnology*, vol. 10, no. 4, p. 308, 2015.
- [9] Y. Zhao, M. Belkin, and A. Alù, "Twisted optical metamaterials for planarized ultrathin broadband circular polarizers," *Nature communications*, vol. 3, p. 870, 2012.
- [10] S. E. Harris, J. E. Field, and A. Imamoglu, "Nonlinear optical processes using electromagnetically induced transparency," *Phys. Rev. Lett.*, vol. 64, pp. 1107–1110, Mar 1990. [Online]. Available: <https://link.aps.org/doi/10.1103/PhysRevLett.64.1107>
- [11] L. V. Hau, S. E. Harris, Z. Dutton, and C. H. Behroozi, "Light speed reduction to 17 metres per second in an ultracold atomic gas," *Nature*, vol. 397, no. 6720, p. 594, Feb 1999.
- [12] M. Lukin and A. Imamoglu, "Controlling photons using electromagnetically induced transparency," *Nature*, vol. 413, no. 6853, p. 273, Mar 2001.
- [13] I. Novikova, R. Walsworth, and Y. Xiao, "Electromagnetically induced transparency-based slow and stored light in warm atoms," *Laser & Photonics Reviews*, vol. 6, no. 3, pp. 333–353, 2012. [Online]. Available: <https://onlinelibrary.wiley.com/doi/abs/10.1002/lpor.201100021>
- [14] Y. Zhang, A. W. Brown, and M. Xiao, "Opening four-wave mixing and six-wave mixing channels via dual electromagnetically induced transparency windows," *Phys. Rev. Lett.*, vol. 99, p. 123603, Sep 2007. [Online]. Available: <https://link.aps.org/doi/10.1103/PhysRevLett.99.123603>
- [15] H. Schmidt and A. Imamoglu, "Giant kerr nonlinearities obtained by electromagnetically induced transparency," *Opt. Lett.*, vol. 21, no. 23, pp. 1936–1938, Dec 1996. [Online]. Available: <http://ol.osa.org/abstract.cfm?URI=ol-21-23-1936>
- [16] R. Yahiaoui, M. Manjappa, Y. K. Srivastava, and R. Singh, "Active control and switching of broadband electromagnetically induced transparency in symmetric metadevices," *Appl. Phys. Lett.*, vol. 111, no. 2, p. 021101, 2017.
- [17] N. Papisimakis, V. A. Fedotov, N. I. Zheludev, and S. L. Prosvirnin, "Metamaterial analog of electromagnetically induced transparency," *Phys. Rev. Lett.*, vol. 101, p. 253903, Dec 2008. [Online]. Available: <https://link.aps.org/doi/10.1103/PhysRevLett.101.253903>
- [18] S. Zhang, D. A. Genov, Y. Wang, M. Liu, and X. Zhang, "Plasmon-induced transparency in metamaterials," *Phys. Rev. Lett.*, vol. 101, p. 047401, Jul 2008. [Online]. Available: <https://link.aps.org/doi/10.1103/PhysRevLett.101.047401>
- [19] R. Singh, C. Rockstuhl, F. Lederer, and W. Zhang, "Coupling between a dark and a bright eigenmode in a terahertz metamaterial," *Phys. Rev. B*, vol. 79, p. 085111, Feb 2009. [Online]. Available: <https://link.aps.org/doi/10.1103/PhysRevB.79.085111>
- [20] C. Wu, A. B. Khanikaev, and G. Shvets, "Broadband slow light metamaterial based on a double-continuum fano resonance," *Phys. Rev. Lett.*, vol. 106, p. 107403, Mar 2011. [Online]. Available: <https://link.aps.org/doi/10.1103/PhysRevLett.106.107403>
- [21] N. Liu, L. Langguth, T. Weiss, J. Kästel, M. Fleischhauer, T. Pfau, and H. Giessen, "Plasmonic analogue of electromagnetically induced transparency at the drude damping limit," *Nature materials*, vol. 8, no. 9, p. 758, 2009.
- [22] F. Hao, Y. Sonnefraud, P. V. Dorpe, S. A. Maier, N. J. Halas, and P. Nordlander, "Symmetry breaking in plasmonic nanocavities: subradiant lsr sensing and a tunable fano resonance," *Nano letters*, vol. 8, no. 11, pp. 3983–3988, 2008.
- [23] M. Manjappa, Y. K. Srivastava, and R. Singh, "Lattice-induced transparency in planar metamaterials," *Phys. Rev. B*, vol. 94, p. 161103, Oct 2016. [Online]. Available: <https://link.aps.org/doi/10.1103/PhysRevB.94.161103>
- [24] S. Xiao, T. Wang, T. Liu, X. Yan, Z. Li, and C. Xu, "Active modulation of electromagnetically induced transparency analogue in terahertz hybrid metal-graphene metamaterials," *Carbon*, vol. 126, pp. 271–278, 2018.
- [25] J. A. Souza, L. Cabral, R. R. Oliveira, and C. J. Villas-Boas, "Electromagnetically-induced-transparency-related phenomena and their mechanical analogs," *Phys. Rev. A*, vol. 92, p. 023818, Aug

2015. [Online]. Available: <https://link.aps.org/doi/10.1103/PhysRevA.92.023818>
- [26] C. L. Garrido Alzar, M. A. G. Martinez, and P. Nussenzveig, "Classical analog of electromagnetically induced transparency," *American Journal of Physics*, vol. 70, no. 1, pp. 37–41, 2002. [Online]. Available: <https://doi.org/10.1119/1.1412644>
- [27] X. Yan, M. Yang, Z. Zhang, L. Liang, D. Wei, M. Wang, M. Zhang, T. Wang, L. Liu, J. Xie *et al.*, "The terahertz electromagnetically induced transparency-like metamaterials for sensitive biosensors in the detection of cancer cells," *Biosensors and Bioelectronics*, vol. 126, pp. 485–492, 2019.
- [28] M. Yang, L. Liang, Z. Zhang, Y. Xin, D. Wei, X. Song, H. Zhang, Y. Lu, M. Wang, M. Zhang *et al.*, "Electromagnetically induced transparency-like metamaterials for detection of lung cancer cells," *Optics express*, vol. 27, no. 14, pp. 19 520–19 529, 2019.
- [29] S. Chen, T. Pan, Y. Peng, G. Yao, M. Gao, and Y. Lin, "Analogue of electromagnetically induced transparency based on bright-bright mode coupling between spoof electric localized surface plasmon and electric dipole," *IEEE Transactions on Microwave Theory and Techniques*, vol. 69, no. 3, pp. 1538–1546, 2021.
- [30] Z. Chen, X. Q. Lin, Y. H. Yan, F. Xiao, M. T. Khan, and S. Zhang, "Noncontact group-delay-based sensor for metal deformation and crack detection," *IEEE Transactions on Industrial Electronics*, vol. 68, no. 8, pp. 7613–7619, 2020.
- [31] J. Zhang, N. Mu, L. Liu, J. Xie, H. Feng, J. Yao, T. Chen, and W. Zhu, "Highly sensitive detection of malignant glioma cells using metamaterial-inspired thz biosensor based on electromagnetically induced transparency," *Biosensors and Bioelectronics*, vol. 185, p. 113241, 2021.
- [32] R. Ning, J. Bao, Y. Meng, and Z. Chen, "Wideband reciprocity tunable electromagnetically induced transparency in complementary graphene metasurface," *Journal of Optics*, vol. 21, no. 4, p. 045106, 2019.
- [33] C. Zhang, Y. Wang, Y. Yao, L. Tian, Z. Geng, Y. Yang, J. Jiang, and X. He, "Active control of electromagnetically induced transparency based on terahertz hybrid metal-graphene metamaterials for slow light applications," *Optik*, vol. 200, p. 163398, 2020.
- [34] L. Han, Q. Tan, Y. Gan, W. Zhang, and J. Xiong, "Polarization-insensitive classical electromagnetically induced transparency metamaterial with large group delay by dirac semimetal," *Results in Physics*, vol. 19, p. 103377, 2020.
- [35] Z. Guo, H. Jiang, Y. Li, H. Chen, and G. Agarwal, "Enhancement of electromagnetically induced transparency in metamaterials using long range coupling mediated by a hyperbolic material," *Optics express*, vol. 26, no. 2, pp. 627–641, 2018.
- [36] D. B. Litt, M. R. Jones, M. Hentschel, Y. Wang, S. Yang, H. D. Ha, X. Zhang, and A. P. Alivisatos, "Hybrid lithographic and dna-directed assembly of a configurable plasmonic metamaterial that exhibits electromagnetically induced transparency," *Nano letters*, vol. 18, no. 2, pp. 859–864, 2018.
- [37] L. Zhu and L. Dong, "Electromagnetically induced transparency metamaterials: theories, designs and applications," *Journal of Physics D: Applied Physics*, vol. 55, no. 26, p. 263003, 2022.
- [38] P. Pitchappa, M. Manjappa, C. P. Ho, Y. Qian, R. Singh, N. Singh, and C. Lee, "Active control of near-field coupling in conductively coupled microelectromechanical system metamaterial devices," *Applied Physics Letters*, vol. 108, no. 11, p. 111102, 2016.
- [39] H. Li, S. Liu, S. Liu, S. Wang, H. Zhang, B. Bian, and X. Kong, "Electromagnetically induced transparency with large delay-bandwidth product induced by magnetic resonance near field coupling to electric resonance," *Applied Physics Letters*, vol. 106, no. 11, p. 114101, 2015.
- [40] X. Su, C. Ouyang, N. Xu, S. Tan, J. Gu, Z. Tian, J. Han, F. Yan, and W. Zhang, "Broadband terahertz transparency in a switchable metasurface," *IEEE Photonics Journal*, vol. 7, no. 1, pp. 1–8, 2015.
- [41] C. Wu, A. B. Khanikaev, and G. Shvets, "Broadband slow light metamaterial based on a double-continuum fano resonance," *Physical review letters*, vol. 106, no. 10, p. 107403, 2011.
- [42] J. Gu, R. Singh, X. Liu, X. Zhang, Y. Ma, S. Zhang, S. A. Maier, Z. Tian, A. K. Azad, H.-T. Chen *et al.*, "Active control of electromagnetically induced transparency analogue in terahertz metamaterials," *Nature communications*, vol. 3, p. 1151, 2012.
- [43] H.-T. Chen, J. F. O'hara, A. K. Azad, A. J. Taylor, R. D. Averitt, D. B. Shrekenhamer, and W. J. Padilla, "Experimental demonstration of frequency-agile terahertz metamaterials," *Nature Photonics*, vol. 2, no. 5, p. 295, 2008.
- [44] M. Manjappa, Y. K. Srivastava, L. Cong, I. Al-Naib, and R. Singh, "Active photoswitching of sharp fano resonances in thz metadevices," *Advanced Materials*, vol. 29, no. 3, p. 1603355, 2017. [Online]. Available: <https://onlinelibrary.wiley.com/doi/abs/10.1002/adma.201603355>
- [45] Q. Xu, X. Su, C. Ouyang, N. Xu, W. Cao, Y. Zhang, Q. Li, C. Hu, J. Gu, Z. Tian *et al.*, "Frequency-agile electromagnetically induced transparency analogue in terahertz metamaterials," *Optics letters*, vol. 41, no. 19, pp. 4562–4565, 2016.
- [46] S. Wang, L. Kang, and D. H. Werner, "Hybrid resonators and highly tunable terahertz metamaterials enabled by vanadium dioxide (vo 2)," *Scientific reports*, vol. 7, no. 1, p. 4326, 2017.
- [47] M. J. Dicken, K. Aydin, I. M. Pryce, L. A. Sweatlock, E. M. Boyd, S. Walavalkar, J. Ma, and H. A. Atwater, "Frequency tunable near-infrared metamaterials based on vo 2 phase transition," *Optics express*, vol. 17, no. 20, pp. 18 330–18 339, 2009.
- [48] W. Cao, R. Singh, C. Zhang, J. Han, M. Tonouchi, and W. Zhang, "Plasmon-induced transparency in metamaterials: Active near field coupling between bright superconducting and dark metallic mode resonators," *Applied Physics Letters*, vol. 103, no. 10, p. 101106, 2013.
- [49] P. Pitchappa, M. Manjappa, C. P. Ho, R. Singh, N. Singh, and C. Lee, "Active control of electromagnetically induced transparency with dual dark mode excitation pathways using mems based tri-atomic metamolecules," *Applied Physics Letters*, vol. 109, no. 21, p. 211103, 2016. [Online]. Available: <https://doi.org/10.1063/1.4969061>
- [50] P. Pitchappa, M. Manjappa, C. P. Ho, Y. Qian, R. Singh, N. Singh, and C. Lee, "Active control of near-field coupling in conductively coupled microelectromechanical system metamaterial devices," *Applied Physics Letters*, vol. 108, no. 11, p. 111102, 2016. [Online]. Available: <https://doi.org/10.1063/1.4943974>
- [51] P. Pitchappa, M. Manjappa, C. P. Ho, R. Singh, N. Singh, and C. Lee, "Active control of electromagnetically induced transparency analog in terahertz mems metamaterial," *Advanced Optical Materials*, vol. 4, no. 4, pp. 541–547, 2016. [Online]. Available: <https://onlinelibrary.wiley.com/doi/abs/10.1002/adom.201500676>
- [52] T. Badloe, J. Lee, J. Seong, and J. Rho, "Tunable metasurfaces: the path to fully active nanophotonics," *Advanced Photonics Research*, vol. 2, no. 9, p. 2000205, 2021.
- [53] D. Qi, K. Zhang, G. Tian, B. Jiang, and Y. Huang, "Stretchable electronics based on pdms substrates," *Advanced Materials*, vol. 33, no. 6, p. 2003155, 2021.
- [54] H. Li, S. Liu, S. Liu, S. Wang, G. Ding, H. Yang, Z. Yu, and H. Zhang, "Low-loss metamaterial electromagnetically induced transparency based on electric toroidal dipolar response," *Applied Physics Letters*, vol. 106, no. 8, p. 083511, 2015.
- [55] P. Tassin, L. Zhang, R. Zhao, A. Jain, T. Koschny, and C. M. Soukoulis, "Electromagnetically induced transparency and absorption in metamaterials: the radiating two-oscillator model and its experimental confirmation," *Physical review letters*, vol. 109, no. 18, p. 187401, 2012.
- [56] S. Han, L. Cong, H. Lin, B. Xiao, H. Yang, and R. Singh, "Tunable electromagnetically induced transparency in coupled three-dimensional split-ring-resonator metamaterials," *Scientific reports*, vol. 6, p. 20801, 2016.
- [57] Y. Tian, S. Hu, X. Huang, Z. Yu, H. Lin, and H. Yang, "Low-loss planar metamaterials electromagnetically induced transparency for sensitive refractive index sensing," *Journal of Physics D: Applied Physics*, vol. 50, no. 40, p. 405105, 2017.
- [58] P. Tassin, L. Zhang, T. Koschny, E. N. Economou, and C. M. Soukoulis, "Low-loss metamaterials based on classical electromagnetically induced transparency," *Phys. Rev. Lett.*, vol. 102, p. 053901, Feb 2009. [Online]. Available: <https://link.aps.org/doi/10.1103/PhysRevLett.102.053901>
- [59] K. Tsakmakidis, L. Shen, S. Schulz, X. Zheng, J. Upham, X. Deng, H. Altug, A. Vakakis, and R. Boyd, "Breaking lorentz reciprocity to overcome the time-bandwidth limit in physics and engineering," *Science*, vol. 356, no. 6344, pp. 1260–1264, 2017.
- [60] Z. Zhao, Y. Chen, Z. Gu, and W. Shi, "Maximization of terahertz slow light by tuning the spoof localized surface plasmon induced transparency," *Optical Materials Express*, vol. 8, no. 8, pp. 2345–2354, 2018.
- [61] F. Zhang, X. He, X. Zhou, Y. Zhou, S. An, G. Yu, and L. Pang, "Large group index induced by asymmetric split ring resonator dimer," *Applied Physics Letters*, vol. 103, no. 22, p. 221904, 2013.
- [62] F. Bagci and B. Akaoglu, "A polarization independent electromagnetically induced transparency-like metamaterial with large group delay and delay-bandwidth product," *Journal of Applied Physics*, vol. 123, no. 17, p. 173101, 2018.
- [63] —, "Single and multi-band electromagnetically induced transparency-like effects with a four-fold symmetric metamaterial design," *Materials Research Express*, vol. 6, no. 5, p. 055806, 2019.

- [64] B. S. Tung, B. X. Khuyen, P. T. Linh, N. T. Tung, D. H. Manh, and V. D. Lam, "Polarization-insensitive electromagnetically-induced transparency in planar metamaterial based on coupling of ring and zigzag spiral resonators," *Modern Physics Letters B*, vol. 34, no. 10, p. 2050093, 2020.
- [65] X. Yin, M. Wu, Y. Liu, and C. Huang, "A planar metamaterial based on metallic rectangular-ring pair for narrow electromagnetically induced transparency-like effect," *Journal of Applied Physics*, vol. 128, no. 6, p. 065105, 2020.